Annals of Nuclear Energy 42 (2012) 35–42

Contents lists available at SciVerse ScienceDirect

Annals of Nuclear Energy

journal homepage: www.elsevier.com/locate/anucene

The mechanical integrity of fuel pin cladding in a pulsed-beam accelerator driven subcritical reactor

Ali Ahmad *, Geoffrey T. Parks

Department of Engineering, University of Cambridge, Cambridge CB2 1PZ, United Kingdom

ARTICLE INFO

Article history:
Received 22 September 2011
Accepted 8 December 2011
Available online 5 January 2012

Keywords:
Accelerator driven subcritical reactor
Fixed field alternating gradient accelerator
Pulsed-beam operation
Thermal cyclic fatigue
Fuel pin cladding integrity

ABSTRACT

The Accelerator Driven Subcritical Reactor (ADSR) is one of the reactor designs proposed for future nuclear energy production. Interest in the ADSR arises from its enhanced and intrinsic safety characteristics, as well as its potential ability to utilize the large global reserves of thorium and to burn legacy actinide waste from other reactors and decommissioned nuclear weapons. The ADSR concept is based on the coupling of a particle accelerator and a subcritical core by means of a neutron spallation target interface. One of the candidate accelerator technologies receiving increasing attention, the Fixed Field Alternating Gradient (FFAG) accelerator, generates a pulsed proton beam. This paper investigates the impact of pulsed proton beam operation on the mechanical integrity of the fuel pin cladding. A pulsed beam induces repetitive temperature changes in the reactor core which lead to cyclic thermal stresses in the cladding. To perform the thermal analysis aspects of this study a code that couples the neutron kinetics of a subcritical core to a cylindrical geometry heat transfer model was developed. This code, named PTS-ADS, enables temperature variations in the cladding to be calculated. These results are then used to perform thermal fatigue analysis and to predict the stress-life behaviour of the cladding.

1. Introduction

Accelerator Driven Subcritical Reactors (ADSR) are one of the possible future fission reactor systems under consideration that target sustainability, enhanced safety and economic competitiveness. In addition, ADSRs can be used to incinerate problematic actinide waste and long-live radiotoxic fission products. Interest in ADSRs also arises from the possibility of deploying thorium in them. The use of thorium in an ADSR was first proposed by Bowman (1998). Thorium is three to four times more abundant in nature than uranium and under certain circumstances produces fewer minor actinides (International Atomic Energy Agency, 2005).

The concept of an ADSR is based on the coupling of a particle accelerator that delivers a beam of protons of about 1 GeV energy to initiate spallation reactions in a heavy metal target and a subcritical reactor fed by the spallation neutrons. The fact that the reactor core is inherently subcritical means that the reactor can be shut down simply by shutting off the accelerator. Among the accelerator technologies under consideration for deployment in an ADSR, the Fixed Field Alternating Gradient (FFAG) concept seems to be a promising candidate (Bungau et al., 2008). The FFAG offers better performance than a cyclotron in terms of its beam characteristics such as beam focusing and rapid acceleration (Mori, 2006). Moreover, FFAGs have a lower construction cost than linear accelerators (Takahashi, 2000). The FFAG was developed for rapid acceleration, which is ideal for systems requiring both high beam power and high repetition rates (Symon et al., 1956). An FFAG accelerator has already been coupled to a reactor core in Kyoto University Research Reactor Institute (KURRI) and studies of its performance conducted (Yamamoto and Shiroya, 2003; Tanigaki et al., 2006). An FFAG delivers accelerated protons in the form of discontinuous bunches, which in an ADSR would result in a pulsed spallation source. This, in turn, would lead to oscillations in the number of fission reactions within the subcritical core and therefore in the core power. Temperatures in the core can, in consequence, also be expected to oscillate.

This paper presents work done in coupling a fuel pin heat transfer model to a neutron kinetics model in order to study the dynamic response of the fuel to pulsed-beam operation in an ADSR. This coupling was required to facilitate thermo-mechanical stress analyses, based on which the consequences of various accelerator beam transients can be quantified. The pulsed-beam delivery in FFAG accelerators will induce cyclic thermal stresses in the fuel pellets and cladding. This study focusses attention on the thermo-mechanical response of the fuel cladding as this is the barrier that prevents fission fragments from leaking into the coolant circuit. As long as the cladding maintains its integrity thermo-mechanical damage to the fuel pellets is of limited significance. The thermally induced stress variation in the cladding will determine the number of allowable cycles, both in normal

* Corresponding author. Tel.: +44 1223 748245; fax: +44 1223 332662.
E-mail address: aa579@cam.ac.uk (A. Ahmad).

0306-4549/$ - see front matter © 2011 Elsevier Ltd. All rights reserved.
doi:10.1016/j.anucene.2011.12.012

Nomenclature

ρ	coolant density (kg m^{-3})
ρ_c	clad density (kg m^{-3})
ρ_f	fuel density (kg m^{-3})
σ_a	stress amplitude
σ'_f	fatigue strength coefficient
A	channel flow area (m^2)
b	Basquin's exponent
C_p	coolant specific heat capacity (J kg^{-1} K^{-1})
C_{pc}	clad specific heat capacity (J kg^{-1} K^{-1})
C_{pf}	fuel specific heat capacity (J kg^{-1} K^{-1})
h_w	clad-coolant heat transfer coefficient (W m^{-2} K^{-1})
h_g	gap heat transfer coefficient (W m^{-2} K^{-1})
K'	cyclic strength coefficient
k_c	clad thermal conductivity (W K^{-1} m^{-1})
k_f	fuel thermal conductivity (W K^{-1} m^{-1})
K_p	fatigue plasticity coefficient
$\dot{m}$	coolant mass flow rate (kg s^{-1})
n_c	number of radial clad nodes
n_f	number of radial fuel nodes
q'	linear heat flux (W m^{-1})
q''	surface heat flux (W m^{-2})
q'''	volume heat flux (W m^{-3})
r_c	clad outer radius (m)
r_f	fuel pellet outer radius (m)
r_g	clad inner radius (m)
T_b	coolant bulk temperature (K)
T_c	clad outer surface temperature (K)

pulsed-beam operation and in the face of the larger transients induced by beam trips. The coupling between models of the reactor neutron kinetics and fuel pin heat transfer was achieved through the development of the PTS-ADS code. This code is described in the next section.

2. The PTS-ADS code

PTS-ADS is a Fortran77 code developed to couple the neutron kinetics of subcritical systems to a fuel pin heat transfer model. The code uses an implicit finite difference method, based on forward time-marching. At present, the code models a single channel in a fast neutron spectrum reactor. The PTS-ADS reactor kinetics are described by a six-group point kinetics model with temperature-to-reactivity feedback included. The single channel heat transfer model consists of a fuel heating model and a heat transfer model from a heated wall to the coolant bulk.

The reactor physics of an ADSR is fundamentally different from that of critical reactors. Its subcriticality has many implications for the neutronic behaviour of the core and thus for reactor control. While the power level of critical reactors depends on the fuel mass present in the core and the deployment of control materials (control rods, soluble boron etc.), the power level in an ADSR depends on the margin of subcriticality and the accelerator beam current. In subcritical reactors the total neutron flux is the summation of the source neutrons, prompt fission neutrons and delayed neutrons. The source neutrons are produced via the spallation process through the interaction between the high energy protons in the accelerator beam and the heavy metal spallation target, and therefore their population is independent of the multiplying medium characteristics. In contrast, the populations of prompt and delayed neutrons depend of the properties of the multiplying medium and the intensity of the source. The neutronic kinetics can be described by a six-group point kinetics model with a time-dependent neutron source. The use of a point kinetics model to describe the physics of ADSRs was successfully demonstrated by Eriksson et al. (2005).

The nominal intensity of the source term when the accelerator beam is on can be calculated based on steady-state operating conditions and power normalisation. When the beam is off, the rate of decay of the neutron population depends strongly on the type of coolant, i.e. whether the ADSR is operating with a fast or thermal neutron spectrum. This translates into different neutron lifetimes in the point kinetics equations.

In general, temperature-to-reactivity feedback effects are not as important in an ADSR as in conventional critical reactors due to the presence of the source neutrons: these reduce the ADSR's sensitivity to reactivity changes. However, when the system is close to criticality, reactivity feedback mechanisms become more significant. Two such mechanisms have been included in the PTS-ADS neutronic model: fuel temperature feedback (Doppler feedback) and coolant density feedback. The former depends on the fuel design and composition; the latter depends on the choice of coolant and flow parameters.

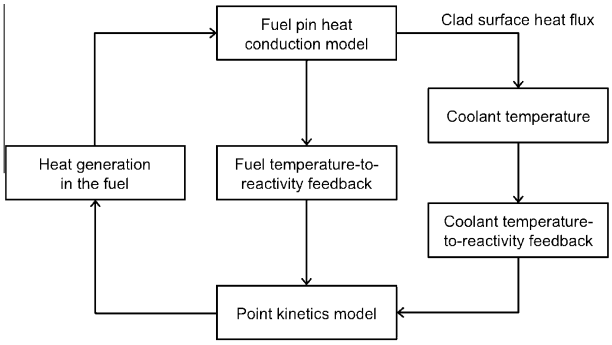

Fig. 1. The PTS-ADS thermo-hydraulic-neutronic coupled model.

2.1. PTS-ADS physical modelling

A flow chart of the PTS-ADS coupled model is shown in Fig. 1. A run starts by calculating the power generated in the fuel from the initial conditions and the temperature distribution in the fuel and clad is obtained by applying the heat conduction model. The corresponding Doppler reactivity feedback is calculated and saved. The coolant bulk temperature is then calculated using the convective heat transfer model with the appropriate heat transfer coefficient correlation. Having determined the coolant temperature, the coolant temperature-to-reactivity feedback can then be calculated. Both reactivity feedbacks are then inserted into the point kinetics model which calculates the power generation in the fuel, and so on.

2.1.1. Fuel pin heat transfer model

The PTS-ADS heat transfer model uses the following assumptions in the computation of the temperature distribution:

- The axial power distribution has a sinusoidal form. [1]

[1] The power distribution in an ADSR depends on the core's effective multiplication factor, but the distribution can be assumed to follow the fundamental harmonic if the system is not highly subcritical (Kadi and Carminati, 2002).

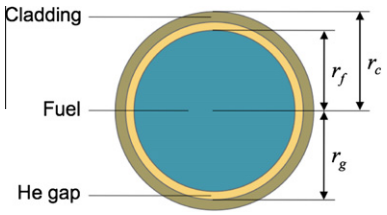

Fig. 2. Fuel rod geometry.

- The heat generation rate is uniform radially across the fuel pin.
- Heat transfer only occurs in the radial direction.

The fuel pin cylindrical geometry is shown in Fig. 2. At each axial step, the model computes the radial temperature distribution by solving the heat transfer equation, which, in cylindrical coordinates, can be written as:

$$\rho C_p \frac{\partial T}{\partial t} - \frac{1}{r}\frac{\partial}{\partial r}\left(rk\frac{\partial T}{\partial r}\right) = Q \tag{1}$$

where Q is the heat source term, k is the thermal conductivity, C_p is the specific heat capacity and ρ is the density of the material.

The boundary conditions are given by:

$$\left(\frac{\partial T}{\partial r}\right)_{r=0} = 0 \tag{2}$$

$$\left(-k_c\frac{\partial T}{\partial r}\right)_{r=r_c} = h_w(T_c(t) - T_b(t)) \tag{3}$$

$$\left(-k_f\frac{\partial T}{\partial r}\right)_{r=r_f} = q''(r_f, t) \tag{4}$$

$$\left(-k_c\frac{\partial T}{\partial r}\right)_{r=r_g} = q''(r_g, t) \tag{5}$$

where the various parameters are defined in the Nomenclature.

To solve the radial heat transfer equation subject to the defined set of boundary conditions (Eqs. (2)–(5)) the finite difference method is used to discretise both the time and space derivatives. The space discretisation is achieved by constructing a radial mesh as shown in Fig. 3.

Using standard methods Eq. (1) can be discretised giving the coefficients for a standard matrix representation as detailed in Appendix A.

2.1.2. Steady-state numerical solution

In steady-state operation, Eq. (1) reduces to:

$$\frac{1}{\rho C_p}\frac{1}{r}\frac{\partial}{\partial r}\left(rk\frac{\partial T}{\partial r}\right) + \frac{1}{\rho C_p}Q = 0 \tag{6}$$

Using the finite difference forms, Eq. (6) becomes in matrix–vector form:

$$\underline{\underline{A}}\,\underline{T} = \underline{B} \tag{7}$$

where $\underline{\underline{A}}$ is a tridiagonal matrix of temperature-dependent coefficients, $\underline{T}$ is the vector of radial temperatures and $\underline{B}$ is the radial heat generation vector:

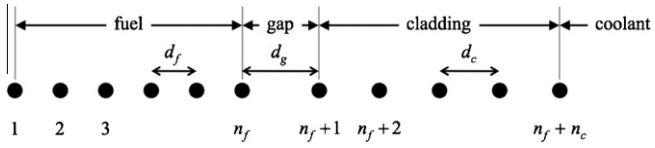

Fig. 3. Fuel rod radial mesh.

$$\underline{\underline{A}} = \begin{bmatrix} b_1 & c_1 & & & & & & \\ a_2 & b_2 & c_2 & & & & & \\ & \ddots & \ddots & \ddots & & & & \\ & & a_i & b_i & c_i & & & \\ & & & \ddots & \ddots & \ddots & & \\ & & & & a_{n_f+n_c-1} & b_{n_f+n_c-1} & c_{n_f+n_c-1} & \\ & & & & & a_{n_f+n_c} & b_{n_f+n_c} \end{bmatrix}; \tag{8}$$

$$\underline{T} = \begin{bmatrix} T_1 \\ \vdots \\ T_{n_f} \\ T_{n_f+1} \\ \vdots \\ T_{n_f+n_c-1} \\ T_{n_f+n_c} \end{bmatrix}; \quad \underline{B} = \begin{bmatrix} -q'''/(\rho_f C_{p_f}) \\ \vdots \\ -q'''/(\rho_f C_{p_f}) \\ 0 \\ \vdots \\ 0 \\ -h_w T_b/(\rho_c C_{p_c}) \end{bmatrix} \tag{9}$$

where the various parameters are defined in the Nomenclature. The coefficients of matrix $\underline{\underline{A}}$ are detailed in Appendix A.

Since the coefficients of matrix $\underline{\underline{A}}$ are variable, Eq. (7) is solved using Newton's iteration method. The solution starts with an initial guess of the radial temperature distribution (for instance, it can be assumed to be uniform and equal to the coolant inlet temperature), then the second distribution is calculated based on the first, the third based on the second and so on. The calculation is halted when convergence is achieved. At each iteration, Eq. (7) is solved using the tridiagonal matrix algorithm, a simplified form of Gaussian elimination (Conte and de Boor, 1980).

2.1.3. Transient numerical solution

Because of its better numerical stability, the implicit method is used for the transient case. The time term in differenced form at node i is:

$$\frac{\partial T}{\partial t} = \frac{T_i^{j+1} - T_i^j}{\Delta t} + O(\Delta t) \tag{10}$$

The matrix form of Eq. (1) can be written as:

$$\underline{T}^{j+1} = \underline{T}^j + \Delta t(\underline{\underline{A}}^{j+1}\underline{T}^{j+1} + \underline{B}^{j+1}) \tag{11}$$

Rearranging, Eq. (11) can be expressed as:

$$\underline{\underline{A}}'\underline{T}^{j+1} = \underline{B}' \tag{12}$$

where

$$\underline{\underline{A}}' = \underline{\underline{I}} - \Delta t\underline{\underline{A}}^{j+1} \tag{13}$$

$$\underline{B}' = \underline{T}^j + \Delta t\underline{B}^{j+1} \tag{14}$$

with $\underline{\underline{I}}$ being the identity matrix.

$\underline{\underline{A}}$ and $\underline{B}$ are the same as in the steady-state case. Eq. (12) is of the same form as Eq. (7) and can therefore be solved in a similar manner.

The coolant bulk temperature T_b is found by solving the following energy equation:

$$C_p\left(\rho A\frac{\partial T_b}{\partial t} + \dot{m}\frac{\partial T_b}{\partial z}\right) = q'(z) \tag{15}$$

where the various parameters are defined in the Nomenclature, with $q'(z)$, the linear heat flux, being:

$$q'(z) = 2\pi r_c h_w(T_{n_f+n_c} - T_b) \tag{16}$$

Eq. (15) can be written in finite difference form as:

$$C_p\rho A\left[\frac{T_{b,l}^{j+1}-T_{b,l}^{j}}{\Delta t}\right]+C_p\dot{m}\left[\frac{T_{b,l}^{j}-T_{b,l-1}^{j}}{\Delta z}\right]=2\pi r_c h_w\left(T_{n_f+n_c,l}^{j}-T_{b,l}^{j}\right) \quad (17)$$

where l is the axial node index. Hence, rearranging Eq. (17):

$$T_{b,l}^{j+1}=T_{b,l}^{j}+\Delta t\left[\frac{2\pi r_c h_w}{C_p\rho A}\left(T_{n_f+n_c,l}^{j}-T_{b,l}^{j}\right)-\frac{\dot{m}}{\rho A\Delta z}\left(T_{b,l}^{j}-T_{b,l-1}^{j}\right)\right] \quad (18)$$

2.1.4. Neutronics model

PTS-ADS uses a point kinetics model with 6 groups of delayed neutrons to calculate the variation of power with time during transients. The mathematical formulation of the model is:

$$\frac{\partial P(t)}{\partial t}=\frac{\rho(t)-\beta}{\Lambda}P(t)+\sum_{i=1}^{6}\lambda_i C_i(t)+S(t) \quad (19)$$

$$\frac{\partial C_i(t)}{\partial t}=\frac{\beta_i}{\Lambda}P(t)-\lambda_i C_i(t) \quad (20)$$

where $P(t)$ is the normalised prompt power, $C_i(t)$ is the population of precursor group i, β is the effective delayed neutron fraction, β_i is the delayed neutron fraction of group i, ρ is the total reactivity, Λ is the prompt neutron generation time, and $S(t)$ is the independent source term.

The total reactivity can be written as:

$$\rho(t)=\rho(0)+\Delta\rho_{fuel}(T_f)+\Delta\rho_{coolant}(T_b) \quad (21)$$

where $\Delta\rho_{fuel}(T_f)$ is the fuel-temperature-to-reactivity feedback, also known as the Doppler reactivity feedback, and $\Delta\rho_{coolant}(T_b)$ is the coolant-temperature-to-reactivity feedback due to the variation in coolant density with temperature.

The finite difference forms of Eqs. (19) and (20) are:

$$\frac{P^{j+1}-P^{j}}{\Delta t}=\frac{\rho(t)-\beta}{\Lambda}P^{j+1}+\sum_{i=1}^{6}\lambda_i C_i^{j+1}+S^{j+1}(t) \quad (22)$$

$$\frac{C_i^{j+1}-C_i^{j}}{\Delta t}=\frac{\beta_i}{\Lambda}P^{j+1}-\lambda_i C_i^{j+1} \quad (23)$$

which can be rearranged to give:

$$P^{j+1}=\frac{P^{j}+\Delta t\sum_{i=1}^{6}\left(\frac{\lambda_i C_i^{j}}{1+\Delta t\lambda_i}\right)+\Delta t S^{j+1}(t)}{1-\Delta t\left(\frac{\rho(t)-\beta}{\Lambda}\right)-\Delta t^2\sum_{i=1}^{6}\left(\frac{\lambda_i\beta_i}{\Lambda[1+\Delta t\lambda_i]}\right)} \quad (24)$$

$$C_i^{j+1}=\frac{C_i^{j}+\Delta t\frac{\beta_i}{\Lambda}P^{j+1}}{1+\Delta t\lambda_i} \quad (25)$$

Using Eq. (24) the normalised power at time step $j+1$ can be calculated based on parameter values from the previous time step, and then the precursor group populations can be updated using Eq. (25).

The initial conditions for this point kinetics model are:

$$P^1=1 \quad (26)$$

$$C_i^1=\frac{\beta_i P^1}{\Lambda\lambda_i} \quad (27)$$

2.2. PTS-ADS validation

The PTS-ADS coupled model has been validated by comparing its predictions for both the steady-state and transient cases to the predictions of three different codes included in a benchmark study on beam interruptions in an accelerator-driven system (D'Angelo et al., 2003; D'Angelo et al., 2004). The benchmark study summarises a comparative analysis of the dynamic response of an ADSR to beam interruptions predicted using a set of ten different codes. The three selected codes for the comparison with PTS-ADS are: TRAC-MOD (Liles, 1982), SAS4ADS (Dagan et al., 2002) and SIMADS (Schikorr, 2002). These three codes represent well the range of data scatter in the benchmark study.

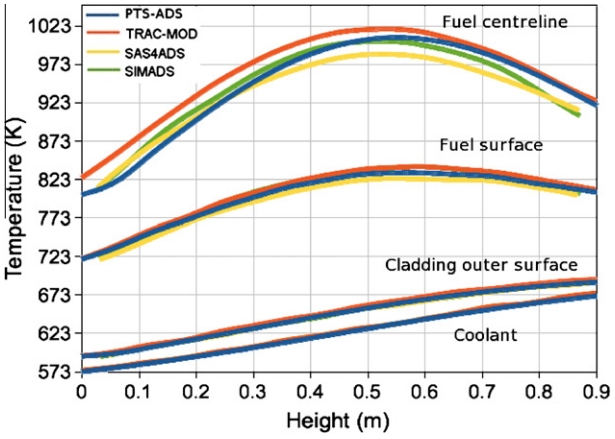

Fig. 4. XADS steady-state axial temperature distributions.

Fig. 4 compares the predictions by the four codes of the axial temperature distributions in the European experimental accelerator-driven system (XADS) and shows good agreement between the PTS-ADS steady-state model and the other three codes. It is clear that the small discrepancies between the codes reduce greatly with distance from the fuel centreline. The focus in this study is on temperature variations in the cladding for which all the codes are in good agreement.

The PTS-ADS neutron kinetics model was tested similarly by comparing its predictions of the magnitude of the normalised power after beam restoration following interruptions of 1, 3, 6 and 12 s to those in the benchmark study produced using the three selected codes. The comparison is shown in Fig. 5. This shows that compared to the other three codes PTS-ADS has slightly over-estimated the peak normalised power reached after long beam interruptions. The difference, however, is less than 2%. Although we have endeavoured to follow the benchmark recommendations as closely as possible, the discrepancy in the peak normalised power in Fig. 5 can be attributed to the effects of slightly different model assumptions or data. The same cause of discrepancies was identified by the participants of the benchmark exercise (D'Angelo et al., 2004).

The same cases were used to validate the PTS-ADS transient thermal model. PTS-ADS predictions of transient temperature variations following beam trips and restorations were compared to those of the three reference codes. Figs. 6 and 7 show these comparisons for the transient variation of the peak fuel centreline temperature and the coolant outlet temperature following a 1 s beam interruption. In both cases it can be seen that the PTS-ADS results agree well with the predictions of the reference codes.

3. Thermo-mechanical response to pulsed operation transients

3.1. Thermal response

The PTS-ADS code was used to calculate the temperature variations in fuel cladding due to pulsed-beam operation. The fuel pin geometry and the physical properties of the fuel, cladding and coolant were taken from the XADS fuel pin design (D'Angelo et al., 2004). The values and correlations of the thermo-physical properties of XADS materials are listed in Table 1. Unlike

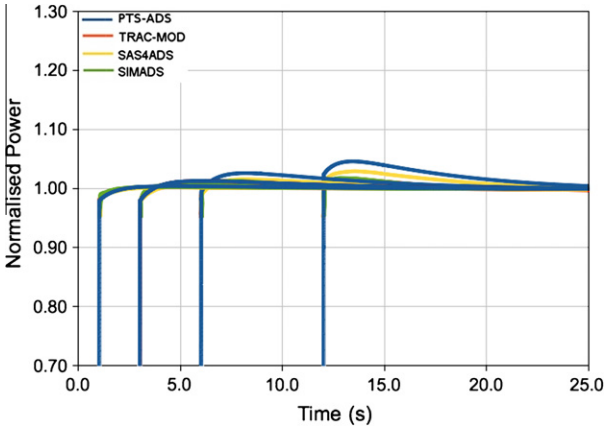

Fig. 5. XADS normalised power transients.

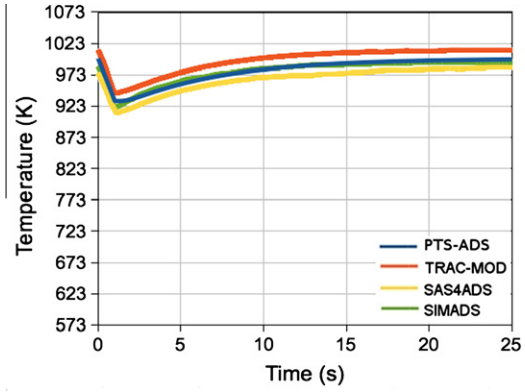

Fig. 6. XADS peak fuel centreline temperature transient induced by a 1 s beam interruption.

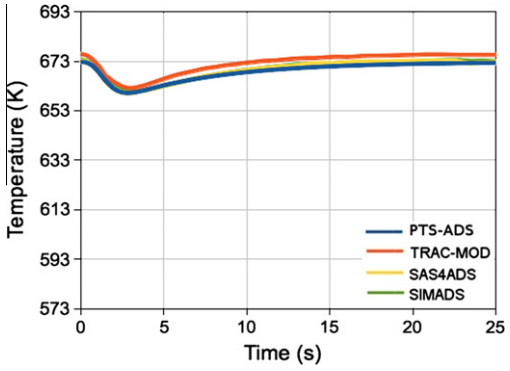

Fig. 7. XADS coolant outlet temperature transient induced by a 1 s beam interruption.

sodium-cooled reactors where the temperature difference between the cladding and the coolant bulk does not normally exceed 10 K, the lower thermal conductivity of lead or lead–bismuth eutectic (LBE), the main coolant candidates for fast ADSRs, increases the clad-coolant temperature difference significantly. Therefore, an appropriate choice of correlation for the heat transfer coefficient is very important. The current version of the PTS-ADS code uses the heat transfer correlation derived by Mikityuk (Pfrang and Struwe, 2007). The adopted correlation works for triangular fuel bundles and represents the best fit of 658 experimental data points.

The neutronic dynamic response to pulsed-beam operation in an ADSR depends on the margin of subcriticality, spatial position in the core and the beam characteristics (Ahmad and Parks, in preparation). For this study, the effective multiplication factor k_{eff} is kept constant and equal to 0.97276, the reference value for XADS, for all cases studied. The effect of the spatial position of the fuel rod can be represented by changing its local power. The accelerator beam characteristics, specifically the beam frequency and beam-off time, play an important role in shaping the neutronic and thermal dynamic response in the core. Since the temperature variations in the cladding due to pulsed-beam operation are expected to be small, the thermal cyclic fatigue is expected to be of a high-cycle nature. The influence of loading frequency is insignificant in the case of high-cycle fatigue conditions in metals (Papakyriacou et al., 2001). Consequently, the choice of the frequency is not important from a thermo-mechanical response perspective. All cases were therefore run with a frequency of 1 Hz. It should be noted, however, that operating an FFAG accelerator at a frequency of 1 Hz would mean a very high instantaneous peak current. One of the advantages of FFAG accelerators is their ability to operate at higher frequencies (up to 1 kHz) than conventional synchrotrons. The use of FFAG technology for ADSR applications is a topic of active research (Tanigaki et al., 2006; Tanigaki et al., 2007) and the optimal values of repetition frequency and beam-off time have not been yet established.

It is expected that the beam-off time of an FFAG will be of the order of 10 ms (Tanigaki et al., 2007). As the beam-off time increases, the magnitudes of the temperature fluctuations in the cladding inner and outer surface increase and the effect of increasing the local linear power becomes more significant. For this study the beam-off time was therefore conservatively estimated to be 100 ms. The linear power corresponding to that of the midplane local power of the XADS fuel rod studied in (D'Angelo et al., 2003) is 9172 W m^{-1}. It was estimated that for an industrial-scale 2 GW(th) power generating ADSR the linear power at midplane would be 25 kW m^{-1}. Fig. 8 shows the variation of the cladding inner surface temperature corresponding to this power rating and a beam-off time of 100 ms. It can be seen that even for this extreme case the magnitude of the temperature oscillation is only about 2 K.

3.2. Cladding thermal stress

During its service, the cladding may suffer from different thermo-mechanical effects such as creep, swelling and embrittlement that influence its mechanical integrity. In the case of a pulsed-beam ADSR, the cyclic variations of the cladding temperature will induce thermal fatigue. The significance of such cyclic behaviour depends on a range of factors such as the physical properties of the cladding material, the amplitude and mean of induced stresses etc.

The total stress loading applied to the cladding during operation is the sum of the mechanical and thermal stresses. The mechanical stress σ_M can be estimated using *Thin Cylinder Theory* (Hearn, 1997) as:

$$\sigma_M = \frac{(p_{gas} - p_h) r_g}{d_c} \tag{28}$$

where p_{gas} is the internal pressure due to fission gases, p_h is the hydrostatic pressure applied on the outer cladding surface, r_g is the cladding inner radius and $d_c = r_c - r_g$ is its thickness. Assuming the net pressure is 1 MPa (Ceballos-Castillo, 2007), the mechanical stress applied to the cladding is 7.522 MPa. The value of applied mechanical stress will not greatly affect the thermal fatigue calculations as the stress variation is only due to that of the thermal stress.

The thermal stress acting on the cladding is caused by the radial temperature gradient between the inner and outer surfaces. During pulsed operation, the temperature gradient will change with time

Table 1
XADS fuel pin material properties (D'Angelo et al., 2003).

Property	Correlation or value
Clad thermal conductivity, k_c	$15.4767 + 0.003448T$ W K^{-1} m^{-1}
Clad density, ρ_c	7924 kg m^{-3}
Clad specific heat capacity, C_{pc}	620 J kg^{-1} K^{-1}
Fuel thermal conductivity, k_f	$[0.042 + 2.71 \times 10^{-4}T]^{-1} + 6.9 \times 10^{-11}T^3$ W K^{-1} m^{-1}
Fuel density, ρ_f	10,354 kg m^{-3}
UO_2 specific heat capacity, C_{pUO_2}	$81.825 + 0.78695T - 1.1552 \times 10^{-3}T^2$ $+9.9037 \times 10^{-7}T^3 - 5.1982 \times 10^{-10}T^4$ $+1.5241 \times 10^{-13}T^5 - 1.7906 \times 10^{-17}T^6$ J kg^{-1} K^{-1}
PuO_2 specific heat capacity, C_{pPuO_2}	$-4.9236 \times 10^6 T^{-2} + 240.89 + 0.32556T$ $-3.5398 \times 10^{-4}T^2 + 1.512 \times 10^{-7}T^3$ $-1.9707 \times 10^{-11}T^4$ J kg^{-1} K^{-1}
Fuel specific heat capacity, C_{pf}	$\frac{214.65}{270.21}C_{pUO_2} + \frac{55.56}{270.21}C_{pPuO_2}$
Coolant density, ρ	$11{,}112 - 1.375T$ kg m^{-3}
Coolant specific heat capacity, C_p	146.5 J kg^{-1} K^{-1}

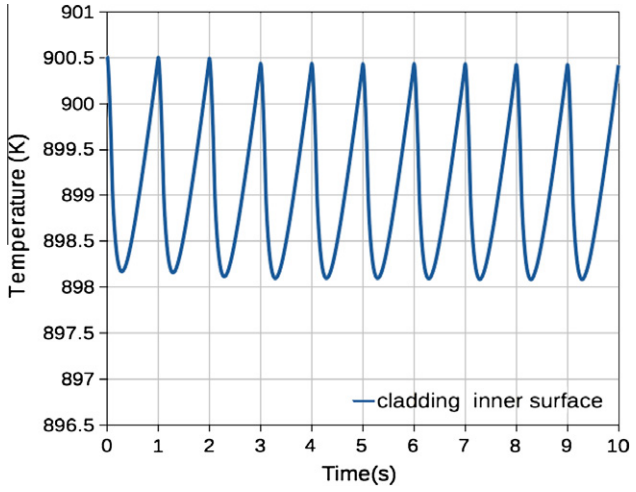

Fig. 8. Cladding inner surface temperature variation due to pulsed operation with 100 ms beam-off time and 1 Hz frequency at 25 kW m^{-1} linear power.

and therefore induce compression and expansion stresses. The thermal stress σ_T applied to the cladding can be estimated using (ASME, 2010):

$$\sigma_T = \frac{E\beta\Delta T}{2(1-\nu)} \tag{29}$$

where E is the Young's modulus of the cladding material, ν is its Poisson's ratio, β is its coefficient of thermal linear expansion, and ΔT is the temperature difference between the cladding inner and outer surfaces. The cladding material used in this study is the same as that intended for XADS: 9Cr-1Mo (T91) steel. T91 steel is one of the proposed structural materials for ADSR applications because of its good thermo-mechanical properties and behaviour under irradiation (Rasche et al., 1992). The mechanical properties of T91 steel used in this study are presented in Table 2.

3.3. Life prediction of fuel pin cladding

The behaviour of fuel pin cladding under pulsed-beam operation can be predicted by relating the amplitude of stress or strain variations to the number of cycles to failure N_f. Since the maximum amplitude of the stress variation in all the cases considered is lower than the yield stress, the fatigue loads are small and the induced strain is elastic. Fig. 9 shows the variation in cladding hoop stress for the same power rating and beam-off time as used in Fig. 8.

The stress amplitude $\Delta\sigma_a = \frac{1}{2}(\sigma_{max} - \sigma_{min})$ is related to N_f by Basquin's law (Basquin, 1910):

$$\Delta\sigma_a = \sigma'_f(2N_f)^b \tag{30}$$

where σ'_f is the fatigue strength coefficient and b is the fatigue strength exponent (Basquin's exponent). For T91 at 300 °C and 550 °C which define the range of the cladding operating temperature, σ'_f and b can be obtained from the data published in (Verleene et al., 2006; Weisenburger et al., 2008) which relate strain rather than stress to the number of allowable cycles. Basquin's exponent b would be the same in both forms. σ'_f can be written as (Troshchenko and Khamaza, 2010):

$$\sigma'_f = K'(K_p)^{n'} \tag{31}$$

where K' is the cyclic strength coefficient, K_p is the fatigue plasticity coefficient, and n' is the cyclic strain hardening exponent. Since the thermal fatigue in the fuel cladding is of high-cycle nature, the effect of the mean stress should be included to improve accuracy. Morrow proposed a modification to the fatigue strength coefficient to account for the effect of the mean stress (Morrow, 1968):

$$\sigma''_f = \sigma'_f - \sigma_m \tag{32}$$

where σ_m is the mean stress.

To account for the effects of local plasticity and creep, a correction factor to the stress amplitude has to be calculated. The method is described in (ASME, 2010). The modified maximum equivalent strain range $\Delta\epsilon_{mod}$ can calculated as:

$$\Delta\epsilon_{mod} = \left(\frac{\sigma^*}{\bar{\sigma}}\right)K^2\Delta\epsilon_{max} \tag{33}$$

where K is either the stress concentration factor or the maximum value of the theoretical elastic stress concentration factor, σ^* is the stress at the maximum strain range, $\bar{\sigma}$ is the stress at a strain range $K\Delta\epsilon_{max}$, and $\Delta\epsilon_{max}$ is the maximum equivalent strain range. For an elastic uniaxial stress, K can be defined as the ratio of the maximum stress to the nominal (mean) stress, that is:

$$K = \frac{\sigma_{max}}{\sigma_m} \tag{34}$$

The strain terms in Eq. (33) can be replaced by the stress divided by Young's modulus, which is assumed to be constant during the stress cycle as the temperature change is relatively small. Eq. (33) can then be written as:

$$\Delta\sigma_{mod} = \left(\frac{\sigma^*}{\bar{\sigma}}\right)K^2\Delta\sigma_a \tag{35}$$

and, as $\bar{\sigma} = K\sigma^*$, simplified to:

Table 2
T91 steel mechanical properties at 300 °C.

Property	Value	Reference
Young's modulus, E	187,900 MPa	Ashrafi-Nik (2006)
Coefficient of thermal linear expansion, β	12.4×10^{-6} K^{-1}	Ashrafi-Nik (2006)
Poisson's ratio, v	0.3	Ashrafi-Nik (2006)
Yield stress, σ_y	440 MPa	Verleene et al. (2006)
Ultimate tensile strength, σ_{TS}	550 MPa	Verleene et al. (2006)

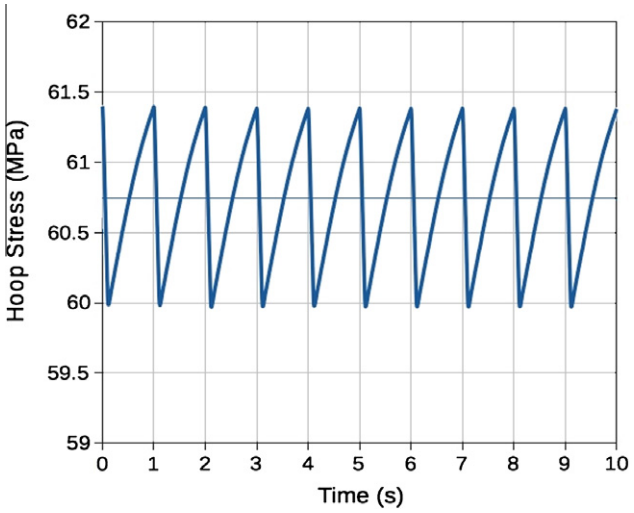

Fig. 9. Cladding hoop stress variation due to pulsed operation with 100 ms beam-off time and 1 Hz frequency at 25 kW m^{-1} linear power.

Table 3
T91 cladding stress-life parameters in an LBE-cooled ADSR.

Temp (°C)	b	σ_m (MPa)	σ_f' (MPa)	σ_f'' (MPa)	$\Delta\sigma_{mod}$ (MPa)	N_f
300	−0.052	29.66	725.26	695.60	0.24	∞
550	−0.093	69.29	719[a]	649.71	0.7	∞

[a] The fatigue strength coefficient at 550 °C was calculated using Mitchell estimation in Troshchenko and Khamaza (2010). The T91 ultimate tensile stress at 550 °C was taken from Chaouadi (2005).

$$\Delta\sigma_{mod} = K\Delta\sigma_a \tag{36}$$

Using the temperature variations estimated by the PTS-ADS code for the defined, conservative ADSR pulsed-beam operating characteristics, the stress-life parameters of T91 fuel cladding in an LBE environment were calculated. These are summarised in Table 3.

The results in Table 3 show that the T91 fuel cladding will preserve its integrity indefinitely in an LBE-cooled 2 GW(th) ADSR when subjected to cyclic temperature variations due to pulsed-beam operation. It should be emphasised that the beam characteristics, in particular the assumed beam-off time, have been chosen conservatively so that the thermal stresses experienced by the cladding are considerably more extreme than are likely to be experienced in practice if FFAG accelerators capable of driving ADSRs are successfully developed.

4. Conclusions

Maintaining the integrity of the fuel pin cladding during its service inside a nuclear reactor is of high importance as the cladding provides a barrier against radioactive fission products and prevents them from leaking out into the primary cooling circuit. Operating an ADSR with a pulsed neutron source is one of the possible scenarios associated with the development and deployment of FFAG accelerator technology. The effect of the temperature fluctuations within the cladding due to such an operational regime was investigated using the PTS-ADS code, which was developed specifically for this purpose. It has been found that, even under very conservative modelling assumptions, the thermal fatigue effects in the cladding are very small and therefore the number of allowable cycles to fatigue failure is so high that the mechanical integrity of the cladding can be assumed to be unaffected by the repetitive temperature variations caused by pulsed-beam operation mode.

5. Future work

The work done in this paper represents a first step towards a greater understanding of the reactor-accelerator coupling in ADSRs. The PTS-ADS code will be used to perform a thermo-mechanical analysis to determine the impact of frequent beam interruptions on the mechanical integrity of the fuel cladding. In contrast to the situation in pulsed-beam operation, the fuel cladding is expected to experience thermal shocks and therefore large stresses during beam interruptions. Another accelerator-induced transient to be looked at is beam overpower where a sudden increase in the beam power can also lead to a thermal shock in the fuel cladding. Additionally, the effects on cladding fatigue damage of operational and design variables, such as irradiation damage, high temperature creep and choice of coolant, will be studied.

The pulsed-beam operation case will be revisited to illustrate the possible use of pulsed operation to measure the reactivity of the core of an ADSR accurately. Previous studies have shown that this is achievable by adopting methods like those mentioned in (Ryves and Scott, 1962) and (Baeten and Ait Abderrahim, 2003). These methods require a change in the neutron flux to be able measure the reactivity. It has been suggested that this could be achieved by relying on accelerator beam interruptions. Pulsed-beam operation, on the other hand, has the potential to provide on-line and continuous core reactivity measurements without the need for frequent, potentially problematic, beam interruptions.

Acknowledgement

The authors thank Dr. Suzanne Sheehy of the STFC Rutherford Appleton Laboratory for her helpful insights into FFAG operation.

Appendix A

$$b_1 = -\frac{4}{d_f^2} y_{f_1} k_f(T_1)$$

$$c_1 = \frac{4}{d_f^2} y_{f_1} k_f(T_1)$$

where $y_{f_i} = [\rho_{f_i} C_{p_{f_i}}]^{-1}$ and $d_f = r_f/n_f$.

For $1 < i < n_f$:

$$a_i = \frac{1}{d_f^2}\frac{r_{i-\frac{1}{2}}}{r_i} y_{f_i} k_f(T_i)$$

$$b_i = -\frac{2}{d_f^2} y_{f_i} k_f(T_i)$$

$$c_i = \frac{1}{d_f^2}\frac{r_{i+\frac{1}{2}}}{r_i} y_{f_i} k_f(T_i)$$

$$a_{n_f} = \frac{1}{d_f^* d_f}\frac{r_{n_f-\frac{1}{2}}}{r_{n_f}} y_{f_{n_f}} k_f(T_{n_f})$$

$$b_{n_f} = -\frac{1}{d_f^*}\frac{1}{r_{n_f}} y_{f_{n_f}}\left[r_{n_f+\frac{1}{2}} h_g + \frac{1}{d_f} r_{n_f-\frac{1}{2}} k_f(T_{n_f})\right]$$

$$c_{n_f} = \frac{1}{d_f^*}\frac{r_{n_f+\frac{1}{2}}}{r_{n_f}} y_{f_{n_f}} h_g$$

where $d_f^* = d_f + \frac{1}{2}d_g, r_{n_f-\frac{1}{2}} = r_{n_f} - \frac{1}{2}d_f, r_{n_f+\frac{1}{2}} = r_{n_f} + \frac{1}{2}d_g$ and $d_g = r_g - r_f$.

$$a_{n_f+1} = \frac{1}{d_c^*}\frac{r_{n_f+1\frac{1}{2}}}{r_{n_f+1}} y_{c n_f+1} h_g$$

$$b_{n_f+1} = -\frac{1}{d_c^*}\frac{1}{r_{n_f+1}} y_{c n_f+1}\left[r_{n_f+1\frac{1}{2}} h_g + \frac{1}{d_c} r_{n_f+\frac{1}{2}} k_c(T_{n_f+1})\right]$$

$$c_{n_f+1} = \frac{1}{d_c^* d_c}\frac{r_{n_f+\frac{1}{2}}}{r_{n_f+1}} y_{c n_f+1} k_c(T_{n_f+1})$$

where $y_{ci} = [\rho_{c_i} C_{p_{ci}}]^{-1}$, $d_c = [r_c - r_g]/n_c$, $d_c^* = d_c + \frac{1}{2}d_g$ and $r_{n_f+1\frac{1}{2}} = r_{n_f+1} + \frac{1}{2}d_c$.

For $n_f + 1 < i < n_f + n_c$:

$$a_i = \frac{1}{d_c^2}\frac{r_{i-\frac{1}{2}}}{r_i} y_{ci} k_c(T_i)$$

$$b_i = -\frac{2}{d_c^2} y_{ci} k_c(T_i)$$

$$c_i = \frac{1}{d_c^2}\frac{r_{i+\frac{1}{2}}}{r_i} y_{ci} k_c(T_i)$$

$$a_{n_f+n_c} = \frac{1}{d_c^2}\frac{r_{n_f+n_c-\frac{1}{2}}}{r_{n_f+n_c}} y_{c n_f+n_c} k_c(T_{n_f+n_c})$$

$$b_{n_f+n_c} = -\frac{1}{d_c}\frac{1}{r_{n_f+n_c}} y_{c n_f+n_c}\left[r_{n_f+n_c} h_w + \frac{1}{d_c} r_{n_f+n_c-\frac{1}{2}} k_c(T_{n_f+n_c})\right]$$

References

Ashrafi-Nik, M., 2006. Thermo hydraulic optimisation of the eurisol ds target. Tech. Rep. TM-34-06-0, Paul Scherrer Institut.

ASME, 2010. ASME Boiler and Pressure Vessel Code, An International Code, Section III, Subsection NH, Appendix T. ASME.

Baeten, P., Ait Abderrahim, H., 2003. Reactivity monitoring in ADS, application to the MYRRHA ADS project. Prog. Nucl. Energy 43, 413–419.

Basquin, O., 1910. The exponential law of endurance tests. Proc. Am. Soc. Test. Mater. 10, 625–630.

Bowman, C., 1998. Accelerator-driven systems for nuclear waste transmutation. Annu. Rev. Nucl. Part. Sci. 48, 505–556.

Bungau, C., Barlow, R., Cywinski, R., Tygier, S., 2008. Accelerator driven systems for energy production and waste transmutation. In: Proc. EPAC 2008, Genoa, Italy, pp. 1854–1856.

Ceballos-Castillo, C., 2007. Multidisciplinary design approach and safety analysis of ADSR cooled by buoyancy driven flows. Ph.D. thesis, Delft University of Technology.

Chaouadi, R., 2005. Flow and fracture behavior of 9%Cr-ferritic/martensitic steels. Tech. Rep. SCK-CEN-R-4122, SCK-CEN.

Conte, S., de Boor, C., 1980. Elementary Numerical Analysis: An Algorithmic Approach, 3rd ed. McGraw-Hill, New York.

Dagan, R., Broeders, C., Struwe, D., Pfrang, W., 2002. SAS4ADS – 3D space time dynamic code system for ADS. Tech. Rep., Jahrestagung Kerntechnik, Stuttgart.

D'Angelo, A., Arien, B., Sobolev, V., Van den Eynde, G., Gabrielli, F., 2003. Benchmark on beam interruptions in an accelerator-driven system final report on phase I calculations. Tech. Rep. NEA/NSC/DOC(2003)17, NEA.

D'Angelo, A., Arien, B., Sobolev, V., Van den Eynde, G., Gabrielli, F., 2004. Benchmark on beam interruptions in an accelerator-driven system final report on phase II calculations. Tech. Rep. NEA/NSC/DOC(2004)7, NEA.

Eriksson, M., Cahalan, J., Yang, W., 2005. On the performance of point kinetics for the analysis of accelerator-driven systems. Nucl. Sci. Eng. 149, 298–311.

Hearn, E., 1997. Mechanics of Materials 1, third ed. Butterworth-Heinemann, Oxford.

International Atomic Energy Agency, 2005. Thorium fuel cycle – potential benefits and challenges. Tech. Rep. IAEA-TECDOC-1450, IAEA.

Kadi, Y., Carminati, F., 2002. Accelerator Driven Systems for Energy Production and Waste Incineration: Physics, Design and Related Nuclear Data. ICTP Lecture Notes Series, vol. 12. International Centre for Theoretical Physics, Trieste, Italy, Chapter: Simulation of Accelerator-Driven Systems.

Liles, D., 1982. TRAC-PF1: an advanced best-estimate computer program for pressurized water reactor analysis. Tech. Rep. LA-TIA-TN-82-1, Los Alamos National Laboratory.

Mori, Y., 2006. FFAG accelerators and their applications. In: Proc. EPAC 2006, Edinburgh, Scotland, pp. 950–954.

Morrow, J., 1968. Fatigue Design Handbook. Society of Automotive Engineers, Philadelphia.

Papakyriacou, M., Mayer, H., Pypen, C.H., Plenk, J., Stanzl-Tschegg, S., 2001. Influence of loading frequency on high cycle fatigue properties of b.c.c. and h.c.p. metals. Mater. Sci. Eng. A308, 143–152.

Pfrang, W., Struwe, D., 2007. Assessment of correlations for heat transfer to the coolant for heavy liquid metal cooled core designs. Tech. Rep. FZKA 7352, Helmholtz Association.

Rasche, C., Bendick, W., Orr, J., 1992. Physical properties, transformation behaviour and microstructure of grade T91. In: The Manufacture and Properties of Steel 91 for the Power Plant and Process Industries, Düsseldorf.

Ryves, T., Scott, M., 1962. Subcritical reactivity measurement by a source-jerk method. J. Nucl. Energy AB16, 455–463.

Schikorr, M., 2002. The transient code system SIM-ADS for solid and fluid-fuelled reactor systems (critical and sub-critical). Tech. Rep., Forschungszentrum Karlsruhe.

Symon, K., Kerst, D., Jones, L., Laslett, L., Terwilliger, K., 1956. Fixed-field alternating-gradient particle accelerators. Phys. Rev. 103, 1837–1859.

Takahashi, H., 2000. The role of the accelerator in energy: recent development of an accelerator-driven systems (ADS). Prog. Nucl. Energy 37, 363–369.

Tanigaki, M., Mori, Y., Inoue, M., Mishima, K., Shiroya, S., 2007. Present status of the FFAG accelerators in KURRI for ADS study. In: Proc. APAC 2007, Indore, India, pp. 803–805.

Tanigaki, M., Mori, Y., Inoue, M., Mishima, K., Shiroya, S., Ishi, Y., Fukumoto, S., Machida, S., 2006. Present status of FFAG accelerators in KURRI for ADS study. In: Proc. EPAC 2006, Edinburgh, Scotland, pp. 2367–2369.

Troshchenko, V.T., Khamaza, L.A., 2010. Strain-life curves of steels and methods for determining the curve parameters. Part 1: conventional methods. Strength Mater. 42, 647–659.

Verleene, A., Vogt, J.-B., Serre, I., Legris, A., 2006. Low cycle fatigue behaviour of T91 martensitic steel at 300 °C in air and in liquid lead bismuth eutectic. Int. J. Fatigue 28, 843–851.

Weisenburger, A., Heinzel, A., Fazio, C., Müller, G., Markow, V., Kastanov, A., 2008. Low cycle fatigue tests of surface modified T91 steel in 10^{-6} wt% oxygen containing $Pb_{45}Bi_{55}$ at 550 °C. J. Nucl. Mater. 377, 261–267.

Yamamoto, A., Shiroya, S., 2003. Study on neutronics design of accelerator driven subcritical reactor as future neutron source, part 2: kinetic characteristics. Ann. Nucl. Energy 30, 1425–1435.